RSC Advances

ROYAL SOCIETY OF CHEMISTRY

www.rsc.org/advances

RSC Advances

RSCPublishing

PAPER

Quantum correction to low-temperature resistivity induced by disorder in $La_{2/3}Sr_{1/3}MnO_3$ –ZrO_2 matrix composites

Cite this: DOI: 10.1039/x0xx00000x

Received 00th January 2014,
Accepted 00th January 2014

DOI: 10.1039/x0xx00000x

www.rsc.org/advances

Yuan Jin,[a] Xiao-Long Qian,[a] Bo Lu,[b] Shi-Xun Cao,[a] and Jin-Cang Zhang,[a,b,c,*]

Low-temperature transport properties were systemically studied for the series of (1-*x*) $La_{2/3}Sr_{1/3}MnO_3$ + *x* ZrO_2 (x = 0, 3%, 6%, and 9%) matrix composites under a weak applied magnetic field from 0 to 1 T. The nanoscaled nonmagnetic ZrO_2 particles which are introduced as a secondary phase has been put into ferromagnetic metal bulk ceramics $La_{2/3}Sr_{1/3}MnO_3$. As the density of ZrO_2 nanoparticles increases, the ferromagnetic ordering of the system will enhance as well as the electric transport at low temperatures. The temperature and weak magnetic field dependences of the resistivity upturns of our samples are in good agreement with a combination of electron-electron interaction and weak localization.

Introduction

The Kondo effect, which arises from the exchange interaction between itinerant conduction electrons and localized spin impurities, leads to anomalous temperature dependences in various physical parameters due to the Fermi-surface effect.[1] It was discovered many years ago in metals with dilute magnetic impurities and had been studied in many strongly correlated systems, such as quantum dots and heavy electron compounds.[2-6] Meanwhile, the resistance minima in low temperature, which attracted scientists wide attention due to the intrinsic physical mechanism of the colossal magnetoresistance system, are typical characteristics of the Kondo effect, have been found in ABO_3-type both polycrystalline and single crystalline systems, especially the wide-bandwidth ferromagnetic metal with a high Fermi-level spin polarization perovskite-type manganites.[7-9] In the ferromagnetic region ($T < T_C$) of perovskite-type manganites, it shows a metallic behavior at low temperatures, but the resistivity does not show a residual resistance behavior for $T \rightarrow 0$.[10-12] So far, in order to explain these interesting and abnormal Kondo-like phenomena in perovskite-type manganites, various models have been proposed in terms of several different mechanism, such as quantum corrections to conductivity effect interaction, spin-polarized tunneling through grain boundaries, and Kondo-like mechanisms due to spin disorder.[13-15] At low temperature, it is well known that the coupling between localized spin and conduction electrons serves as a fundamental model for understanding correlated electron physics and it is said that the research about the low-temperature resistivity minima is still under debating. In the past decade, several papers have been published claiming the presence of weak localization and electron-electron (e-e) interaction in the low-temperature region of the magnetotransport properties which give rise to resistivity minimum, ρ_{min}, below nearly about 40 K.[16-20] The e-e interaction mainly exists in the strongly correlated systems and the weak localization is a quantum correction due to the finite dimension of the system as quantum interference between backscatter waves and propagating waves.[12] Rozenberg *et al.*[19] predicted the low-temperature resistivity minima occurs at low temperatures shifts towards lower T upon applying a magnetic field and disappears at some critical field H_{cr}. Xu *et al.*[13] investigated the behavior of the resistivity minimum with various magnetic fields at low temperature for the optimal doped $La_{2/3}Ca_{1/3}MnO_3$ polycrystal and the experimental results did not support the shift of low-temperature resistivity minima and the field H_{cr}, they found weak localization is suppressed by high field (H > 1 T) and the electrical resistivity only follows $T^{1/2}$ dependence with a characteristics of enhanced e-e interaction in 3D disorder systems under high field (H > 1 T). Jia *et al.*[20] investigated the effects of the ferroelectric poling-induced strain on the sputtered $La_{0.7}Ca_{0.15}Sr_{0.15}MnO_3$ films and interpreted the resistivity upturn in terms of quantum correlation originating enhanced by disorder. However, from the experiments, most obtained results include various factors above and strongly depend on the single experimental sample's form. Thus, it is very important to investigate intrinsically the different and single factor such as disorder which is related to the low-temperature resistivity minimum under weak magnetic field.

Perovskite-type manganites have manifested a strong coupling between the spin, charge, orbital and lattice degree of freedom, which lead to a series of novel phenomena for the electronic transport.[21-26] $La_{2/3}Sr_{1/3}MnO_3$ (LSMO) is a wide-bandwidth ferromagnetic metal with a high Fermi-level spin polarization.[27-30] In order to clarify the physical mechanism of the resistivity minimum ρ_{min} in magnetic ordered systems LSMO and to find out the role of spin-dependent effects

associated with ρ_{min}, we introduce ZrO_2 which is an insulator as a secondary phase into the ferromagnetic metal ground state LSMO. ZrO_2 is a versatile electron-doped semiconductor material with a direct wide band gap of 5-7 eV.[31-32] The goal of this work is the experimental study and theoretical description of the influence on disorder in bulk scattering portion of the low-temperature resistivity measured at zero and low magnetic field H (H < 1 T) on a series of (1-*x*) LSMO + *x* ZrO_2 (*x* = 0, 3%, 6%, and 9%) matrix composites samples. As the density of nonmagnetic disorder ZrO_2 increases, not only the ferromagnetic ordering of the system increase, but a higher quantum correlation to resistivity is also measured arising from the increase of the number of ZrO_2. Our results provide experimental confirmation of the weak localization and e-e interaction effect in ferromagnetic oxide materials with nonmagnetic disorder.

Experimental

The matrix composites of (1-*x*)LSMO + *x*ZrO_2 (*x*=0, 3%, 6% and 9%) were prepared by the standard solid state reaction method. Polycrystalline sample of LSMO was prepared by mixing the heat treating stoichiometric quantities of high purity La_2O_3 (99.99%), $SrCO_3$ (99%), and MnO_2 (99%), the raw materials were mixed, palletized and sintered at 1000°C for 12 h, 1200°C for 24 h and 1350°C for 24 h with intermediate grinding and repelletizing. Finally, the obtained powders of LSMO were mixed with volume density of 3%, 6%, and 9% nanoparticle ZrO_2 precipitates respectively. To avoid reaction of LSMO plus ZrO_2, we choose the lower sintered temperature and shorter sintered time. Therefore, the composite mixtures were ultimately pressed into pellets and sintered at 1180 ℃ for 10 h to yield the final composites.

The phase of these samples was characteristic by powder X-Ray diffraction experiments conducted on the Rigaku D/max-2550 diffractometer (18 KW, Cu-*Kα*) at room temperature in the 2θ range of 10° - 80° with a step of 0.02°. The surface morphology was observed by scanning electron microscopy (SEM). The transport and magnetic properties were measured by the Physical Property Measurement System (PPMS-9) made by Quantum Design. Temperature dependence of resistivity was using standard DC four-probe method under various DC magnetic fields of 0 T, 0.05 T, 0.2 T and 1 T. Silver paint was used to make electrical contacts on the samples and the electrical leads were Copper wires.

Results and discussion

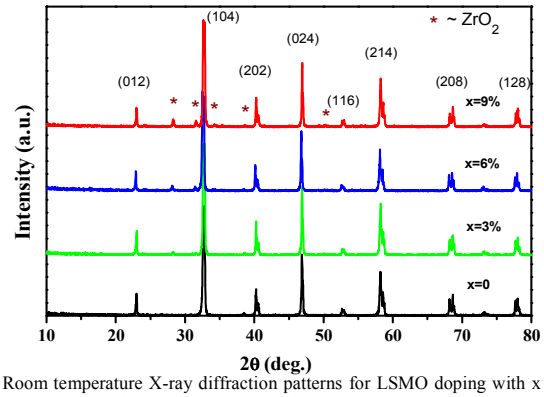

Fig. 1 Room temperature X-ray diffraction patterns for LSMO doping with x = 0, 3%, 6%, and 9% ZrO_2. The brown star symbols represent the peaks of ZrO_2 in X-ray diffraction.

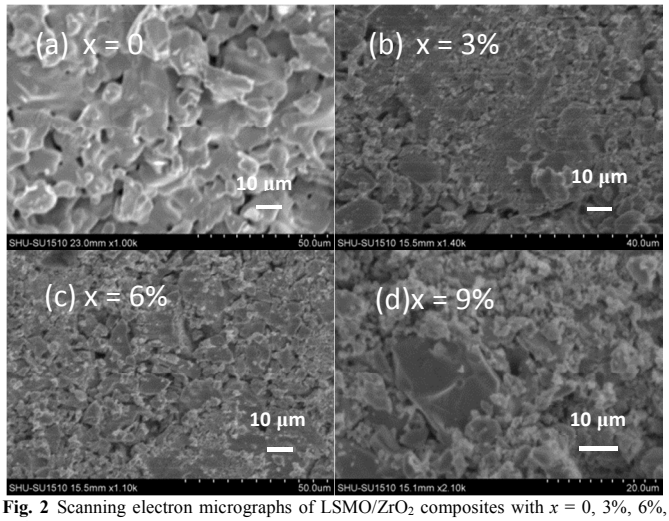

Fig. 2 Scanning electron micrographs of LSMO/ZrO_2 composites with *x* = 0, 3%, 6%, and 9%

The room temperature powder XRD patterns of experimental samples for the series of *(1-x)*LSMO+*x*ZrO_2 (*x* = 0, 3%, 6%, and 9%) matrix composites are shown in Fig. 1. It shows that the spectra are well characterized. It also can be seen that LSMO and nonmagnetic oxides are compatible with each other, indicating no observable chemical reaction between LSMO and nonmagnetic oxides ZrO_2 during the final calcination.

The representative SEM micrographs of *(1-x)*LSMO+*x*ZrO_2 matrix composites with *x* = 0, 3%, 6%, and 9% are shown in Fig. 2, respectively. SEM of all the composites was taken in order to obtain an idea about the distribution of ZrO_2 in LSMO. It is obvious that the smaller size grains of ZrO_2 are randomly distributed in the surrounding of the larger size LSMO grains.

The temperature dependence of the magnetization *M* of the matrix composites is presented in Fig. 3. The inset of Fig. 3 shows the Curie-Weiss fit for the T_C of LSMO, which according to the Curie-Weiss law at $1/M = 0$, the obtained Curie temperature T_C = 371 K, while LSMO with 0, 3%, 6%, and 9% ZrO_2 additions have the same T_C. However, with increasing density of ZrO_2 nanoparticles, ferromagnetic moment increases. We have calculated the full width at half maximum (FWHM) of matrix composites peaks from XRD results, and found that the FWHM value is getting smaller with increasing density of ZrO_2 nanoparticles, which can be considered as a little ZrO_2 nanoparticle will modulate the lattice of ferromagnetic LSMO and make the LSMO grain quality better.

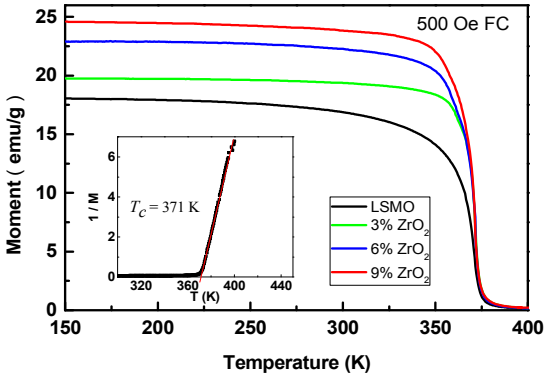

Fig. 3 The temperature dependence of the magnetization for LSMO with x = 0, 3%, 6%, and 9% ZrO_2.

In order to reveal the origin of the resistivity minimum and clarify the influence of nonmagnetic ZrO_2 disorders in the system, the electrical transport properties at low temperature were studied in detail. For better and clearly comparison to reveal the abnormal low-temperature transport behavior, a normalized resistivity by dividing the raw resistivity at temperature of 50 K is showed in Fig. 4. Insets of Fig. 4 plot the raw electrical resistivity behaviour at low temperature on an enlarged scale, from 3 K to 50 K under various fields. As the density of ZrO_2 increases, a higher resistivity is measured. For all the samples, we found the electrical resistivity minimum phenomenon appearing below 30 K and the minimum of electrical resistivity at low temperatures are the typical characteristics of the Kondo-like effect. Moreover, it is worth noting that, the resistivity upturn is strongly enhanced by the applied magnetic field and T_{min} shifts to a lower temperature.

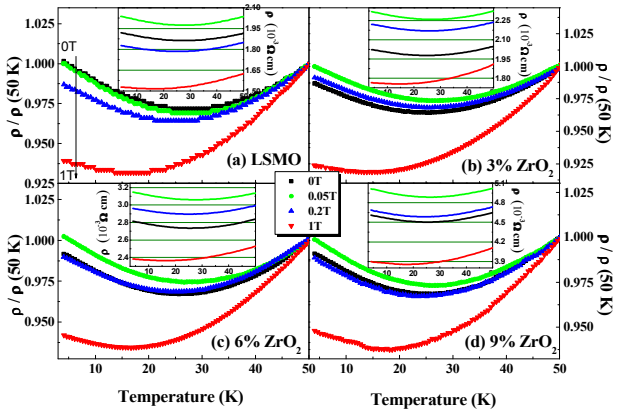

Fig. 4 The temperature dependence of the normalized resistivity $\rho(T) / \rho(50\ K)$ under various applied fields between 0 T and 1 T at a low-temperature enlarge scale for LSMO with x = 0, 3%, 6%, and 9% ZrO_2. Insets show the raw resistivity $\rho(T)$ of the composites under various magnetic fields below 50 K.

We analyze these abnormal phenomena by theoretical methods. Firstly, the total resistivity of the system in the first-order correction can be given by the following expression:

$$\rho = \rho_0 + \rho_m(T, H) - \rho_0^2[\sigma_{ee}(T, H) + \sigma_{wl}(T, H)]. \quad (1)$$

where the $\rho_m(T, H)$ is the magnetic resistivity contributed from the anisotropic MR and magnon scattering.

Based on the strong correlated effect in manganites, the conductivity of the e-e interaction which insensitive to the applied magnetic field can be described as,[19, 21]

$$\sigma_{ee}(T, H) = \sigma_0 + 0.0309\frac{e^2}{\hbar L_T}, \quad (2)$$

where $L_T^{-1} = \sqrt{k_B T/\hbar D} = \beta\sqrt{T}$ is the diffusion length of thermally excited carriers and D is the carrier diffusion constant.

Then, according to the theory of Ziese[12] and Lee[21], the formula for conductivity correction due to contribution of weak localization is,

$$\sigma_{wl}(T, H) = \sigma_0 + \frac{e^2}{\hbar(2\pi)^2}(L_H + lnL_\varphi), \quad (3)$$

where $L_H = \sqrt{\hbar c/eH}$ is the magnetic length, and L_φ is the phase relaxation length due to CI has been obtained by M. Auslender et al.[17] and E. Rozenberg et al.[19] given by $L_\varphi^{-2} = \frac{\gamma e^2}{\hbar} L_T^{-3}$.

Therefore, we can easily find out that the resistivity will drop down and the ρ_{min} of resistivity will decrease with the external magnetic field increase via Eq. (2) and (3), so the total resistivity at these temperatures can be represented can be expressed as,

$$\rho = \rho_0 + \alpha T^5 - \beta\sqrt{T} + \lambda lnT. \quad (4)$$

In this equation, the first term is the residual resistivity, the second term is the inelastic scattering which is independent with the external fields H, the third term is due to the e-e interaction, and the fourth term is due to the weak localization. Using Eq. (4), the fitted temperature dependence of the normalized resistivity under magnetic fields 0 and 0.2 T is shown in Fig. 5 (a) – (d). The results agree well with the experimental data and the corresponding coefficients values are shown in Table 1 as well.

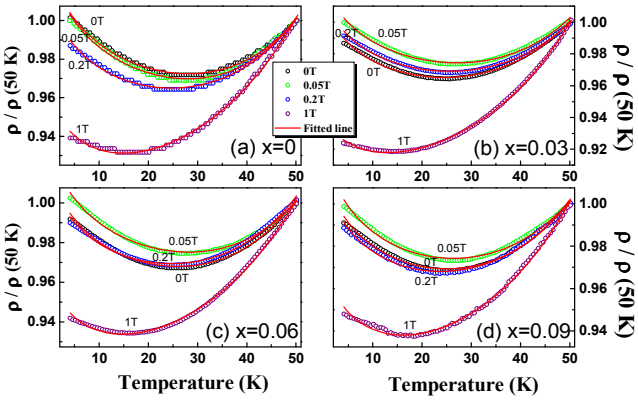

Fig. 5 The resistivity as a function of temperature at the range of 3 K – 50 K under 0, 0.05, 0.2, and 1 T field for LSMO with x = 0, 3%, 6%, and 9% ZrO_2. The symbols are LSMO experimental data and the red dashed line fits to Eq. (4).

Table I. The fitting parameters of Eq. (4) for LSMO with x = 0, 3%, 6%, and 9% nanoscaled nonmagnetic ZrO_2 particles.

	H = 0					H =0.2 T				
	ρ_0 ($10^{-3}\Omega$cm)	β ($10^{-5}\Omega$cm K$^{-1/2}$)	λ ($10^{-5}\Omega$cm K$^{-1/2}$)	D (10^{-2} cm^2/s)	$N(E_F)$ (10^{41} J^{-1}cm^{-3})	ρ_0 ($10^{-3}\Omega$cm)	β ($10^{-5}\Omega$cm K$^{-1/2}$)	λ ($10^{-5}\Omega$cm K$^{-1/2}$)	D (10^{-2} cm^2/s)	$N(E_F)$ (10^{41} J^{-1}cm^{-3})
0	1.10	0.13	0.16	2.35	7.84	1.09	0.16	0.13	1.39	13.81
3%	1.09	0.16	0.15	2.42	6.62	1.09	0.15	0.11	2.33	6.85
6%	1.10	0.16	0.13	4.31	2.58	1.08	0.13	0.09	5.33	2.26
9%	1.08	0.15	0.12	9.68	0.80	1.08	0.12	0.08	15.72	0.48

Fig. 5 (a)-(d) presents the fitting results of the low-temperature resistivity of our system under various magnetic fields. The fitted values under 0 and 0.2 T are presented in Table I, meanwhile, using the Einstein formula $\sigma_0 = e^2N(E_F)D$, the values of electron diffusion constant D and density of Fermi energy state $N(E_F)$ are calculated and shown in Table I.[33-35] We now discuss the fitting parameters in Table I. It is worth to note that under zero fields, fitting data reveal an independence of normalized ρ_0 with ZrO_2 mixing increase, which implies ρ_0 is irrelevant to the low-temperature resistivity upturn. However, the increase of parameter β represents the e-e interaction means the e-e interaction is enhanced by disorder. The value of D for LSMO is much smaller than normal metals [e.g., Cu ($D_{Cu} \approx 2.2\times10^2$ cm^2/s)], which indicates that LSMO has a lower diffusivity than metals. Meanwhile, the value of electron diffusion constant D increase while density of electronic state $N(E_F)$ decrease with increasing of ZrO_2-mixing under zero and an applied magnetic field, which indicates that nonmagnetic disorder can lead to a change in the density of state near the Fermi energy due to e-e interaction. Therefore, the e-e interaction enhanced by disorder is an intrinsic characteristic and verifies the strong correlated interaction between electrons in LSMO system. It determines the resistivity upturn at low temperature.

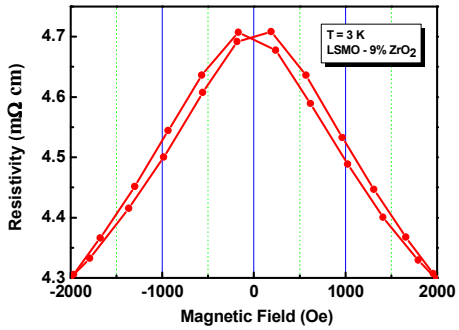

Fig. 6 The resistivity as a function of applied magnetic fields at 3 K for LSMO-9%ZrO_2 on an enlarge scale for the case of low fields.

Then, we pay our attention on the role of intergrain tunneling effect in LSMO-9%ZrO_2. It will affect the $N(E_F)$ under a low magnetic field of the system. Nonmagnetic disorder ZrO_2 acts as a barrier for spin-polarized tunneling between adjacent LSMO grains. Since the double exchange mechanism responsible for metallic conduction in LSMO and nonmagnetic disorder ZrO_2 will enhance ferromagnetic ordering of ferromagnetic ground state system, grain boundary induced by ZrO_2 disorder-introduced will rebuild the original Mn-O-Mn bond angle under H = 0 T, namely, disorder will weaken the double exchange and lead to an increase in resistivity. Our experimental results show in Fig. 6 gives the low field *R-H* curve of LSMO-9%ZrO_2 to illustrate the magnetoresistance hysteretic for the intergrain tunneling effect. In weak magnetic fields, the spins of LSMO magnetic domain will align and spin polarized carriers will increase which will lead to the inelastic scatter and weak localization decrease. Thus, at low fields, the e-e interaction and weak localization decrease can be considered as intergrain tunneling effects which will make the resistivity upturn weaken. Therefore, the abnormal transport behavior in manganites at low temperatures can be understood taking account both e-e interaction and weak localization affected by the grain boundary effect.

Conclusions

In summary, the low-temperature transport properties and its dependence on weak magnetic fields of LSMO introduced by different concentration (0, 3%, 6%, and 9%) nonmagnetic ZrO_2 nanoparticle disorders were systemically studied. The results show that with increasing the density of ZrO_2 nanoparticles, the ferromagnetic ordering of the system will enhance as well as the resistivity at low temperatures. The temperature and weak magnetic field dependence of the resistivity of our samples are in good agreement with a combination of e-e interaction and weak localization. In particular, the fitting results present the e-e interaction enhanced by disorder. While at low fields, the e-e interaction and weak localization decrease can be considered as intergrain tunneling effects. Our results prove that the existence of Kondo-like transport where ferromagnetic ground state manganites mixing with nonmagnetic disorder at low temperature is depending on both weak localization and e-e interaction. Also, to thoroughly understand this unique behavior, more experiments on heterostructure samples and theoretical works are needed.

Acknowledgements

We are grateful to Yu-Ze Gao and Xiao-Peng Cui for their loads of helpful and useful advices. This work is supported by the National Natural Science Foundation of China (NSFC, No. 11074163, 50932003), the Science and Technology Innovation Fund of the Shanghai Education Committee (No.12ZZ097). Experiments are partially supported from Analysis & Measurement Center and Laboratory for Microstructures of Shanghai University.

Notes and references

[a] *College of Science, Shanghai University, Shanghai 200444, China.* Fax/Tel: +86-21-66161146; E-mail: jczhang@shu.edu.cn.
[b] *Laboratory for Microstructures, Shanghai University, Shanghai 200444, China.*
[c] *Materials Genome Institute, Shanghai University, Shanghai 200444, China.*

1 J. Kondo, *Prog. Theo. Phys.*, 1964, **32**, 37-49.
2 A. J. Millis, *Nature*, 1998, **392,** 147-150.
3 K. Katoh, T. Komeda, and M. Yamashita, *J. Chem. Soc., Dalton Trans*, 2010, **39**, 4708–4723.
4 S. Singh and S. K. Dhar, *Phys. Rev. B: Condens. Matter Mater. Phys.*, 2003, **68,** 144433.
5 T. Kubo,Y. Tokura and S. Tarucha, *Phys. Rev. B: Condens. Matter Mater. Phys.*, 2011, **83,**115310.
6 G. Singh-Bhalla, S. Selcuk, T. Dhakal, A. Biswas, and A. F. Hebard, *Phys. Rev. Lett.*, **102**, 2009, 077205.
7 J. C. Zhang, Y. Xu, S. X. Cao, G. X. Cao, Y. F. Zhang and C. Jing, *Phys. Rev. B: Condens. Matter Mater. Phys.*, 2005, **72,** 054410.
8 S. Stølen, E. Bakkenw, and C. E. Mohn, *Phys. Chem. Chem. Phys.*, 2006, **8**, 429–447.

9 Z. H. Zeng, F. Calle-Vallejo, M. B. Mogensenc, and J. Rossmeisl, *Phys. Chem. Chem. Phys.*, 2013, **15**, 7526.
10 Z. Chen, Y. Xu, Y. Su, S. Cao, and J. Zhang, *J. Supercond. Novel Magn.*, 2009, **22**, 465-469.
11 F. A. Rabuffetti and R. L. Brutchey, *J. Chem. Soc., Dalton Trans*, 2014, **43**, 14499-14513.
12 M. Ziese, *Phys. Rev. B: Condens. Matter Mater. Phys.*, 2003, **68**, 132411.
13 Y. Xu, J. C. Zhang, G. X. Cao, C. Jing, and S. X. Cao, *Phys. Rev. B: Condens. Matter Mater. Phys.*, 2006, **73**, 224410.
14 L. J. Ding, K. L. Yao and H. H. Fu, *Phys. Chem. Chem. Phys.*, 2011, **13**, 328–336.
15 Y. Z. Gao, G. X. Cao, J. C. Zhang, and H. U. Habermeier, *Phys. Rev. B: Condens. Matter Mater. Phys.*, 2012, **85**, 195128.
16 C. Barone, A. Guarino, A. Nigro, A. Romano, and S. Pagano, *Phys. Rev. B: Condens. Matter Mater. Phys.*, 2009, **80**, 224405.
17 M. Auslender, A. E. Karkin, E. Rozenberg, and G. Gorodetsky, *J. Appl. Phys.*, 2001, **89**, 6639-6641.
18 X. Y. Feng, W. Q. Chen, J. H. Gao, Q. H. Wang, and F. C. Zhang, *Phys. Rev. B: Condens. Matter Mater. Phys.*, **81**, 2010, 235411.
19 E. Rozenberg, M. Auslender, I. Felner, and G.Gorodetsky, *J. Appl. Phys.*, **88**, 2000, 2578-2582.
20 R. R. Jia, J. C. Zhang, R. K. Zheng, D. M. Deng, H. U. Habermeier, H. L. W. Chan, H. S. Luo, and S. X. Cao, *Phys. Rev. B: Condens. Matter Mater. Phys.*, 2010, **82,** 104418.
21 P. A. Lee and T. V. Ramakrishnan, *Rev. Mod. Phys.* 1985, **57,** 287-337.
22 S. Jin, T. H. Tiefel, M. McCormack, R. A. Fastnacht, R. Ramesh, and L. H. Chen, *Science*, 1994, **264**, 413-415.
23 R. Mahendiran, A. Maignan, S. Hébert, C. Martin, M. Hervieu, B. Raveau, J. F. Mitchell, and P. Schiffer, *Phys. Rev. Lett.*, 2002, **89**, 286602.
24 H. J. Kitchen, I. Saratovsky and M. A. Hayward, *J. Chem. Soc., Dalton Trans*, 2010, **39**, 6098–6105.
25 L. Maritato, C. Adamo, C. Barone, G. M. De Luca, A. Galdi, P. Orgiani, and A. Yu. Petrov, *Phys. Rev. B: Condens. Matter Mater. Phys.*, 2006, **73**, 094456.
26 J. S. Lee, D. A. Arena, P.Yu, C. S. Nelson, R. Fan, C. J. Kinane, S. Langridge, M. D. Rossell, R. Ramesh and C. C. Kao, *Phys. Rev. Lett.* 2010, **105**, 257204.
27 R. A. De Souza, M. S. Islamb and E. Ivers-TiVe, *J. Mater. Chem.*, 1999, **9**, 1621–1627.
28 J. H. Park, E. Vescovo, H. Kim, C. Kwon, R. Ramesh and T. Venkatesan, *Nature*, 1998, **392**, 794-796.
29 D. Niebieskikwiat, L. E. Hueso, J. A. Borchers, N. D. Mathur and M. B. Salamon, *Phys. Rev. Lett.*, 2007, **99**, 247207.
30 R. Epherre, C. Pepin, N. Penin, E. Duguet, S. Mornet, E. Pollert, and G. Goglio, *J. Mater. Chem.*, 2011, **21**, 14990–14998.
31 M. Zheng, Q. Zhu, X. Y. Li, X. M. Li, and R. K. Zheng, *RSC Adv.*, 2014, **4**, 32622–32627.
32 S. Benfer and E. Knozinger, *J. Mater. Chem.*, 1999, **9**, 1203–1209.
33 D.V. Lang, X. Chi, T. Siegrist, A.M. Sergent, and A. P. Ramirez, *Phys. Rev. Lett.*, 2004, **93**, 086802.
34 S. Pisana, S. Costea, T. Kosteski, W. T. Shmayda, N. P. Kherani, and S. Zukotynski, *J. Appl. Phys.*, 2005, **98**, 093705.
35 A. H. Reshak and *S. Azam*, *Int. J. Electrochem. Sci.*, 2013, **8**, 10396.

Quantum correction to low-temperature resistivity induced by disorder in $La_{2/3}Sr_{1/3}MnO_3$ –ZrO_2 matrix composites

Yuan Jin,[a] Xiao-Long Qian,[a] Bo Lu,[b] Shi-Xun Cao,[a] and Jin-Cang Zhang,[a,b,c,*]

Low-temperature transport properties were systemically studied for the series of (1-*x*) $La_{2/3}Sr_{1/3}MnO_3$ + *x* ZrO_2 (x = 0, 3%, 6%, and 9%) matrix composites under a weak applied magnetic field from 0 to 1 T. The nanoscaled nonmagnetic ZrO_2 particles which are introduced as a secondary phase has been put into ferromagnetic ground state metal $La_{2/3}Sr_{1/3}MnO_3$. The temperature and weak magnetic field dependences of the resistivity upturns of our samples are in good agreement with a combination of electron-electron interaction and weak localization.